

Dynamics of the Ly α and C IV emitting gas in 3C 273

Stéphane Paltani

Harvard-Smithsonian Center for Astrophysics, 60 Garden St., Cambridge, MA 02138, USA

spaltani@cfa.harvard.edu

and

Marc Türlér

INTEGRAL Science Data Centre, ch. d'Ecogia 16, CH-1290 Versoix, Switzerland
and

Geneva Observatory, ch. des Maillettes 51, CH-1290 Sauverny, Switzerland

Marc.Turler@obs.unige.ch

ABSTRACT

In this paper we study the variability properties of the Lyman α and C IV emission lines in 3C 273 using archival IUE observations. Our data show for the first time the existence of variability on time scales of several years. We study the spatial distribution and the velocity field of the emitting gas by performing detailed analyses on the line variability using correlations, 1D and 2D response functions, and principal component analysis. In both lines we find evidence for two components, one which has the dynamic properties of gas in Keplerian motion around a black hole with a mass of the order of $10^9 M_{\odot}$, and one which is characterized by high, blue-shifted velocities at large lag. There is no indication of the presence of optically thick emission medium neither in the Ly α , nor in the C IV response functions. The component characterized by blue-shifted velocities, which is comparatively much stronger in C IV than in Ly α , is more or less compatible with being the result of gas falling towards the central black hole with free-fall acceleration. We propose however that the line emission at high, blue-shifted velocities is better explained in terms of entrainment of gas clouds by the jet. This gas is therefore probably collisionally excited as a result of heating due to the intense infrared radiation from the jet, which would explain the strength of this component in C IV relative to Ly α . This phenomenon might be a signature of disk-jet interaction.

Subject headings: Line: profiles – Quasars: emission lines – Quasars: individual: 3C 273 – Ultraviolet: galaxies

1. Introduction

The presence of broad emission lines is a very distinctive feature of quasi-stellar objects (QSOs) and Seyfert 1 galaxies. These lines are emitted by gas located in the vicinity of the central engine photoionized by the strong ionizing continuum radiation. The large width of the emission lines requires velocities well in excess of $10\,000\text{ km s}^{-1}$. Line profile and relative intensity studies provide very important clues on the gas velocity distribu-

tion and on the physical conditions in the line emitting region (e.g., Sulentic et al. 2000).

A huge amount of information can however be gathered by studying the variability properties of the emission lines. Because line emission is driven by the variable continuum from the central engine, the broad emission lines vary in response to the continuum variations. As different parts of the line emitting region respond with different delays depending on their locations, variability can be used

as a tool to map the entire gas phase-space distribution (Blandford & McKee 1982). This provides very important insights on the global dynamics of the system, and much effort has been devoted to the development of analysis methods of emission line light curves (e.g., Dietrich 1995). A very important recent result is the fact that the large emission line widths are to a large extent due to Keplerian motions around supermassive objects, and that this effect provides a way to estimate black hole masses (Peterson & Wandel 1999).

3C 273 is a quite peculiar radio-loud QSO that exhibits, depending on the wavelength domain, the properties of both blazars and Seyfert 1 galaxies (Courvoisier 1998). It has been intensively observed throughout the electromagnetic spectrum for more than 3 decades as part of a large collaboration (Türler et al. 1999), and in particular throughout the mission of the International Ultraviolet Explorer (IUE) satellite, which can observe at wavelengths close to the ionizing continuum, and is particularly well adapted to the study of important emission lines like Ly α (for sufficiently redshifted objects) and C IV.

In this paper, we extend a previous study of the ultraviolet and optical continuum emission (Paltani et al. 1998), and focus on the Ly α and C IV emission line variability based on archival IUE spectra of 3C 273. Previous works on Ly α variability in 3C 273 provided conflicting results. While O’Brien et al. (1989) and O’Brien & Harries (1991) detected significant line variability, Ulrich et al. (1993) found no compelling evidence of variability. These studies used only a part of the entire IUE data set; we add here about 5 years of data, which doubles the period of time with dense sampling. With the addition of these new data, Ly α variability is now clearly detected, and an analysis of C IV is even possible. Moreover, the sampling is now sufficient to perform detailed analyses of the light curves, which allow us to attempt to constrain the geometry and the velocity field of the emitting gas.

Throughout this paper, the quoted wavelengths are observed wavelengths, while the Doppler velocities and the time lags are expressed in the rest frame of 3C 273, i.e. corrected for a redshift of $z=0.158$.

2. Data

This paper is based on data from the 3C 273 database hosted by the Geneva Observatory¹ and presented in Türler et al. (1999). The data that are used here are the IUE short wavelength (SWP) spectra processed with the IUE Newly Extracted Spectra (INES) software (Rodríguez-Pascual et al. 1999). The sample consists of sparse observations from 1978 until 1985, followed by ten years with an observation rate of about once every 2 weeks during two annual observation periods of 3 months, separated by 2 months. Two SWP observations were often performed consecutively to improve photometric accuracy. In total, 256 SWP observations have been performed on 142 different days.

2.1. Spectra selection

Since the inclusion of low quality spectra adds noise or even spurious features to the results, we apply strict selection criteria. We first reject the small aperture spectra and those flagged as dubious in Türler et al. (1999), to which must be added the SWP46739LL spectrum, because of absence of guiding during the exposure. Considering only the ranges between 1260 and 1560 Å for Ly α , and between 1680 and 1980 Å for C IV, we discard spectra clearly contaminated by cosmic rays, those with 10 or more saturated spectral bins at the top of Ly α , as well as those with a signal-to-noise ratio (S/N) below 15 on average.² The last two selection criteria are similar to the rejection of over- and under-exposed spectra applied by O’Brien et al. (1989) and O’Brien & Harries (1991). To ensure that differences between Ly α and C IV are not due to a different sampling, we use an identical set of spectra for both lines.

As in those previous two studies, we correct for the IUE wavelength scale uncertainty by applying small wavelength shifts (≤ 3 Å) to the 186 remaining spectra. Overlooking this point can introduce spurious asymmetric line variability, and can change the line profile in the rms spectrum (see Sect. 2.3). The wavelength correction has been calculated by placing the Gaussian fitted peak of

¹Web site: <http://obswww.unige.ch/3c273/>

²Although it does not satisfy this criterion, SWP19731LL was not discarded, because it is the only spectrum between mid-1982 and mid-1984.

the Ly α line at its expected rest wavelength of 1407.7 Å. Finally, after averaging all spectra taken within 12 hours, we end up with a set of 119 good quality SWP spectra of 3C 273.

2.2. Line flux extraction

The Ly α λ 1216 flux (including N V λ 1240) is measured relative to a continuum defined by a straight line fitted to the points in two 50 Å continuum bands at 1260–1310 and 1510–1560 Å. We integrate the total line flux for Doppler velocities up to 20 000 km s⁻¹, i.e. from 1314 to 1501 Å. The C IV λ 1549 flux was measured similarly, with the continuum bands at 1680–1730 and 1940–1980 Å. To avoid strong contamination by He II λ 1640, we integrate C IV only for velocities up to 10 000 km s⁻¹, i.e. from 1732 to 1851 Å, the observed line center being at \sim 1791.4 Å. Unfortunately, this wavelength is nearly coincident with an IUE reseau mark. In the three spectra taken before 1980, this mark results in a very clear absorption-like feature, that we correct by interpolating linearly above the affected wavelength bins.

The line flux uncertainty is calculated by taking into account both the flux error in each spectral bin and an estimate of the uncertainty induced by the fit to the continuum. As the resolution of IUE is about 6 Å and the spectral bins are \sim 1.7 Å wide, the spectral bins are not completely independent. We take this into account by multiplying the uncertainty resulting from the individual flux errors by $\sqrt{6/1.7} \simeq 1.9$. It can be very easily seen that the uncertainty induced by the fit is expressed as $(\Delta\lambda/2) \sqrt{\sigma_1^2 + \sigma_2^2}$, where $\Delta\lambda = \lambda_2 - \lambda_1$ is the wavelength range of line integration and σ_1, σ_2 are the continuum fit uncertainties at λ_1, λ_2 . We also extract a continuum flux averaged over the 1250–1300 Å range. The same provision for non-independent spectral bins is taken to estimate the continuum flux uncertainty.

The average uncertainties obtained with the above method are respectively 2% for the continuum, and 3.5% for Ly α and C IV. However, a *structure function analysis* (e.g., Paltani 1999) gives average uncertainties exceeding the above ones by factors 1.6, 1.2, and 2 respectively. This means that the INES uncertainties are slightly underestimated (which we have confirmed using a single-bin, continuum light curve). We therefore apply these correction factors to our continuum,

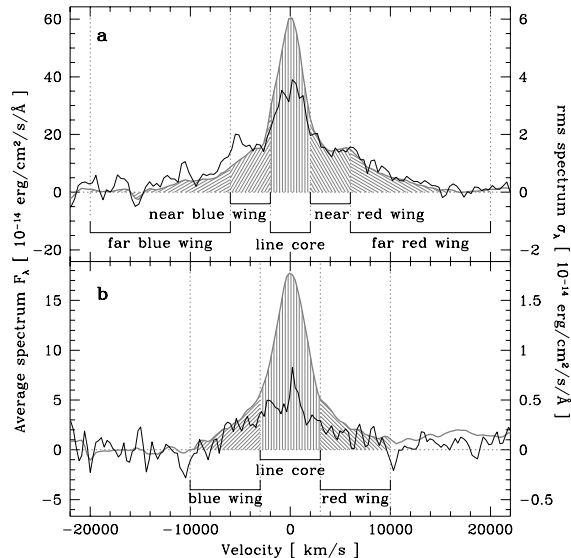


Fig. 1.— Average Ly α (a) and C IV (b) line (grey solid line) and rms profiles (black solid line). For better comparison the rms profile is shown on a ten times larger scale. The definition of the different parts of the lines are also shown.

Ly α , and C IV light curves. We finally obtain average uncertainties of 3.5%, 4.5%, and 7%, respectively.

2.3. Average and rms line profiles

In Fig. 1a we compare the average Ly α emission line profile and the root-mean-square (rms) profile. The rms profile is defined as in Wandel et al. (1999). The rms Ly α profile is comparably broader than the average profile, which indicates that the wings of this line are much more variable than its core. Another significant difference is an excess in the blue wing variability (around -5000 km s⁻¹). The contamination of Ly α by the N V λ 1240 line in its red wing (around $+5000$ km s⁻¹) is visible, but relatively small. The C IV rms profile shows similar features, but with a lesser S/N.

2.4. Light curves

The light curves of the integrated Ly α and C IV lines and of the ultraviolet continuum (1250–1300 Å) are shown in Fig. 2 and printed in Table 1 (published in full in the Electronic Version). They

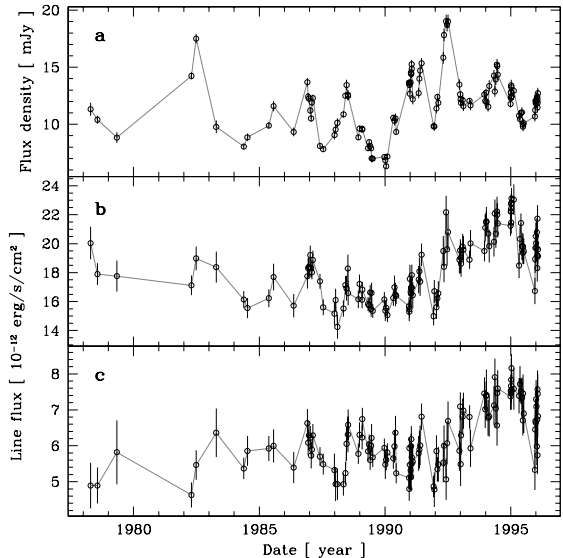


Fig. 2.— (a) Ultraviolet continuum light curve averaged in the 1250–1300 Å band. (b) Ly α emission line light curve integrated for velocities up to 20 000 km s $^{-1}$. (c) C IV emission line light curve integrated for velocities up to 10 000 km s $^{-1}$.

can be obtained from the Geneva Observatory web site <http://obswww.unige.ch/3c273/>. Both lines appear to be clearly variable, as confirmed by the large reduced chi-square values of $\chi^2_\nu \simeq 10.3$ for Ly α and $\chi^2_\nu \simeq 4.6$ for C IV obtained under the hypothesis that the line flux is constant (118 degrees of freedom).

The peak-to-peak variability of the Ly α light curve is $\sim 50\%$ of the mean line flux ($\sim 60\%$ for C IV). This is about three times the value found by Ulrich et al. (1993), whose study could not benefit from the data obtained after July 1992. The relative variability, defined as the ratio of the standard deviation corrected for the average uncertainty to the mean flux (Clavel et al. 1991), is 0.11 for Ly α , 0.12 for C IV, and 0.21 for the continuum.

Visual comparison between Figs 2a, 2b, and 2c shows that the Ly α and C IV light curves vary on significantly longer time scales than the continuum, one huge bump lasting at least 4 years dominating the line variability. On short time scales however, the continuum and line light curves are quite similar, as each peak in the line light curves can be found in the continuum.

The average post-1992 line flux is significantly higher than that observed until then. This variability on long time scales could not be observed in previous studies (i.e. O’Brien et al. 1989; O’Brien & Harries 1991; Ulrich et al. 1993), only based on earlier data. As a consequence, this study can explore new facets of (in particular) Ly α emission properties.

3. Correlation analysis

We perform cross-correlation analyses with our data using two different methods: the interpolated cross-correlation function method (ICCF; Gaskell & Peterson 1987) as implemented by White & Peterson (1994), and the z -transformed discrete correlation function (ZDCF) (Alexander 1997). The presence of a period with poor sampling (before 1985) can in principle strongly affect the ICCF because of interpolation. We checked however that the effect is negligible in our case by comparing the ICCFs of the full data set with those using only post-1985 data. We therefore keep below the full set of data for consistency with the other analyses presented here.

Fig. 3 shows the correlation between the 1250–1300 Å continuum and the Ly α and C IV emission lines obtained with the two methods. The agreement is very good, except for a strange dip at a lag of slightly more than 2 years in the ZDCF with Ly α . The significance of the departure of the correlation point at lag 2.36 yr from the ICCF is however only about 2σ .

Qualitatively, the correlations exhibit a rapid increase of the correlation for $\tau > 0$, as expected if the lines are driven by the UV continuum. The peaks are however extremely broad, the correlations returning to zero only at a lag of almost 4 yr. Fig. 3 can be compared to Fig. 9c of Koratkar & Gaskell (1991). Their cross-correlation drops to zero after a bit more than one year, much more rapidly than what we observe. This discrepancy is assuredly the result of the fact that long-time scale variability was absent (or negligible) in the data set they have used. Kaspi et al. (2000), whose data set consists essentially of post-1992 observations, find a closer, but still smaller, value of about 3 yr for H α , H β , and H γ . It can be noted however that these low-ionization lines are expected to lie farther away from the central engine than Ly α and

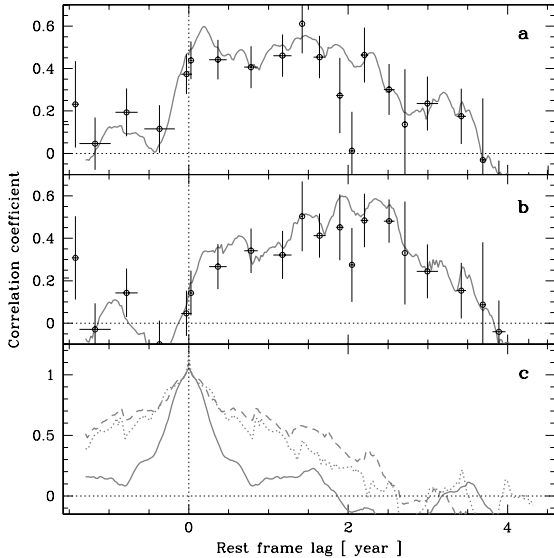


Fig. 3.— (a) and (b) Correlations between the UV 1250-1300Å continuum emission and the Ly α (a), and C IV (b) emission lines. The solid line is the ICCF. The points are the ZDCF. (c) ACFs of the continuum (solid line), Ly α (dashed line), and C IV (dotted line) emission lines. For better comparisons, ACFs are corrected for the effect of uncertainties (see text).

C IV.

An interesting difference between the cross-correlations with Ly α and C IV is that the cross-correlation is markedly lower for lags smaller than 0.5 yr in the case of C IV. In particular, the peak at 0.2 yr visible in the Ly α ICCF is completely absent in the C IV ICCF. The correlation at 0 lag is about 0.1 for C IV, compared to more than 0.4 for Ly α . The other parts of the correlations are very similar in both lines.

If two time series are causally related by a response function (see Sect. 4), the width of the correlation peak is due in part to the response function, and in part to the autocorrelation of the driving time series (technically, the correlation is the convolution of the autocorrelation with the response function). It is therefore important to test whether the broad correlation peaks in Figs 3a and b could be due to the autocorrelation of the ultraviolet continuum. Fig. 3c shows the autocorrelation functions (ACFs) of the continuum, Ly α ,

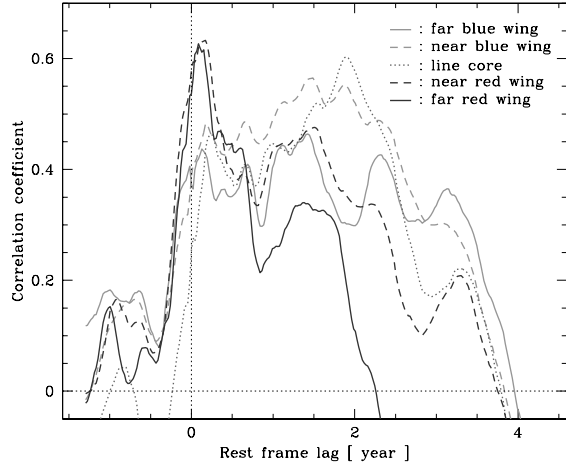


Fig. 4.— ICCF correlations between the UV 1250-1300Å continuum emission and the five parts of the Ly α emission line as defined in Fig. 1.

and C IV light curves calculated using the same method as the ICCFs. To get rid of the effect of uncertainties, which makes comparisons between ACFs difficult, we normalized the autocorrelations so that they equal 1 for a very small non-null lag $\tau = 0.04$ yr. The UV continuum ACF shows a very narrow central peak with a FWHM of about 0.6 yr, dropping to almost 0 at $\tau \simeq 0.75$ yr. This shows that the correlations are to a large extent dictated by the response function. Fig. 3c also shows the ACFs of the two lines. They exhibit much broader FWHMs of the order of 3 yr. The Ly α ACF is a little bit broader than that of C IV, but the significance of this result is questionable.

To gain insight into the dynamics of the line-emitting region, we decompose the Ly α and C IV emission lines into respectively 5 and 3 parts as defined in Fig. 1. For Ly α , the line core is defined as the part of the line with absolute velocities smaller than 2000 km s $^{-1}$. The near wing (either red or blue) is defined by absolute velocities between 2000 and 6000 km s $^{-1}$. The far wing (again red or blue) extends from absolute velocities of 6000 km s $^{-1}$ up to 20 000 km s $^{-1}$ (The choice of 6000 km s $^{-1}$ distributes more or less evenly the contamination by NV in the near and far red wings). Because of S/N limitations, we could not use the same velocity boundaries for C IV. We define the C IV line core as the part of the line with absolute velocities up to 3000 km s $^{-1}$, the rest be-

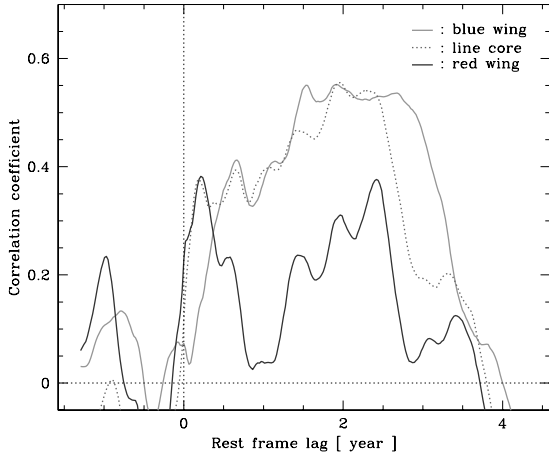


Fig. 5.— ICCF correlations between the UV 1250-1300Å continuum emission and the three parts of the C IV emission line as defined in Fig. 1.

ing respectively the blue and red wings. Table 2 shows the relative variability of the different parts of the Ly α and C IV lines. In both lines, the blue part varies significantly more than the red one, or that the core.

Fig. 4 shows the ICCFs between the ultraviolet continuum and the five parts of Ly α defined above. A very moderate smoothing of the curves at large lag has been applied in this figure for clarity. The major difference is that both the ZDCF and the ICCF for the far red wing decrease much faster than those with the other parts of the line, reaching 0 correlation at a lag close to 2 yr instead of 4. A faster decrease in correlation for the near red wing is also observed, although it is marginal in the ICCF. These results indicate that the Ly α blue wing varies on time scales significantly longer than the red wing. Another difference is that the peak at very small lag is only present in the red wing. It must be noted however that this excess of correlation is not at all compelling in the ZDCFs.

The correlations of the ultraviolet continuum with the different parts of the C IV line (Fig. 5) also show a faster drop of correlation in the red wing, although the correlation has a quite peculiar shape. The much smaller correlation at very small

lag is here also mostly contained in the red wing of the line.

4. Response function analysis

4.1. 1D and 2D response functions

It is well known that the emission line variations in Seyfert galaxies follow those of the ultraviolet continuum (e.g., Peterson 1998). This is naturally explained in models where gas in the periphery of an active galactic nucleus (AGN) is illuminated by the ultraviolet radiation from the central engine. As the gas responds to the continuum variation with a delay depending on its location, we can write the relationship between the overall emission line flux $F_L(t)$ and the continuum flux $F_C(t)$ in the form of the following convolution (Krolik & Done 1995):

$$F_L(t) = \langle F_L \rangle + \int_{-\infty}^{+\infty} \Psi(\tau) \cdot [F_C(t-\tau) - \langle F_C \rangle] d\tau, \quad (1)$$

where $\Psi(\tau)$ is the 1-dimensional response function, depending on τ only, and is mostly defined by the geometry of the line emitting region; and $\langle x \rangle$ denotes the time average of the variable x . Note that the form of Eq. (1) allows for arbitrary non-linear relationship between $F_L(t)$ and $F_C(t-\tau)$, provided it can be locally approximated by a linear relationship for variations of F_C around $\langle F_C \rangle$.

Solving Eq. (1) for $\Psi(\tau)$ can in principle provide very strong constraints on the BLR geometry. We perform this deconvolution using the regularized linear inversion deconvolution method, first applied to AGN reverberation studies by Krolik & Done (1995), one of the standard methods described by Horne (1999): We first transform the deconvolution into a set of linear equations, which is in general very ill-conditioned. We sample the response function with a higher time resolution for $\tau \leq 1$ yr. To avoid completely unstable solutions, a matrix imposing the smoothness of the solution is added to the matrix representing the convolution. Several kinds of smoothing matrices can be chosen. We opt here for the simplest one, which imposes a constant solution on the equation system. By increasing the weight of the smoothing matrix, one can get arbitrarily smooth solutions. On the other hand, setting the weight to 0 removes all smoothing, and the method becomes equivalent

to a singular value decomposition. By convention, a weight of 1 means that the trace of the convolution matrix and that of the smoothing matrix are identical. Throughout the paper, we adopt a weight of 5. No additional smoothing is applied. All numerical integrations are made using a simple trapezoidal formula. Technical details on the method can be found in Press et al. (1992).

Eq. (1) gives the relation between the continuum and the total line flux. However, we can alternatively define a response function for each particular velocity v . This gives the 2-dimensional response function $\Psi(\tau, v)$, which relates the line and continuum fluxes according to the following equation:

$$F_L(t, v) = \langle F_L(v) \rangle + \int_{-\infty}^{+\infty} \Psi(\tau, v) \cdot [F_C(t-\tau) - \langle F_C \rangle] d\tau \quad (2)$$

2D response functions of BLRs in AGN have been studied theoretically by several authors (e.g., Blandford & McKee 1982; Welsh & Horne 1991; Pérez et al. 1992; O’Brien et al. 1994), but, to our knowledge, only Wanders et al. (1995) (to a limited extent) and Ulrich & Horne (1996) have attempted to derive them from actual observations. In practice, we integrate $F_L(t, v)$ over velocity bins of width 500 km s^{-1} close to the center of the line and up to 2000 km s^{-1} in the outer wings, and replace Eq. (2) by a small number of independent equations having the form of Eq. (1). We use the same regularized linear inversion method to solve these equations.

4.2. Results

Fig. 6 shows the 1D response functions and the reconstructed $\text{Ly}\alpha$ and C IV light curves resulting from the convolution of the UV continuum with the response function. We choose the smoothing weight so as not to wash out the features in the response that appear robust (i.e. those that are present over a large range of weights, namely roughly from 1 to 50). The reconstructed light curve matches reasonably well the original light curves, although the effect of measurement uncertainties is quite obvious in the case of C IV . We also checked that the stability of the response function is very good when its time sampling is modified, and when a few points are removed from the light curves.

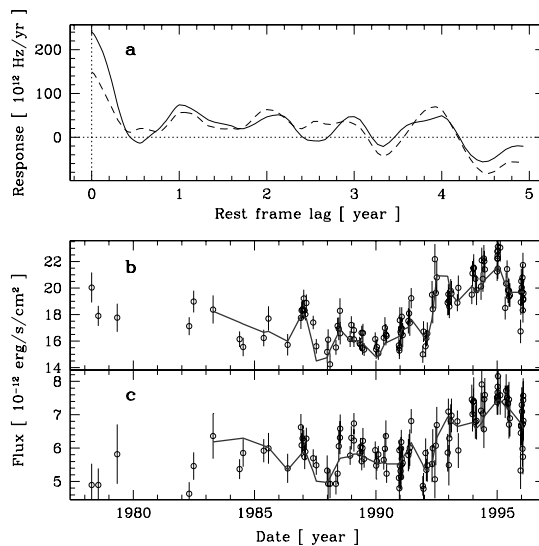


Fig. 6.— (a) Response function linking the $\text{Ly}\alpha$ (solid line) and C IV (dashed line) emissions to the $1250\text{-}1300 \text{ \AA}$ UV continuum. The C IV response has been multiplied by a factor 3. (b) Comparison between the $\text{Ly}\alpha$ light curve (points) and the UV continuum convolved with the above response function (solid line). (c) Same as (b) for the C IV emission line.

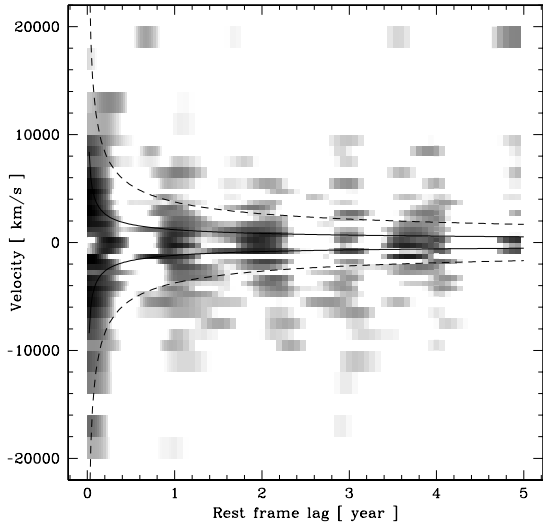


Fig. 7.— 2D response function of the Ly α emission line. Response below a given threshold is indicated by a white zone; black zones indicate highest response. The lines are the envelopes of the response function for a Keplerian circular velocity field around a black hole of $10^8 M_\odot$ (solid lines) and $10^9 M_\odot$ (dashed lines) respectively.

The response functions of both line light curves are mainly characterized by a quite prominent peak at 0 lag which vanishes for $\tau \simeq 0.5$ yr, followed by evidence of significant response up to $\tau \simeq 4$ yr. It must be noted that the significance of the structures in the response function, like the bumps and hollows, is difficult to assess and will therefore be left out of our discussion. The CIV response function differs mostly from that of Ly α in the ratio between the response at small lags $\tau \leq 0.5$ yr and that at longer lags $\tau \geq 0.5$ yr. This ratio is about twice lower in CIV than in Ly α .

Fig. 7 shows the 2D response function of the Ly α emission line (we did not attempt to calculate the 2D response function for CIV, because of the poorer S/N). The most obvious result is the very broad response up to $\tau \simeq 0.4$ yr. The bumps of Fig. 6 are clearly visible, and have also markedly narrower extent in velocity, as expected if their widths are due to Keplerian motion around a massive object (i.e., $v \sim r^{-1/2}$). A third feature in Fig. 7 is a clear excess of response at lag $\tau \geq 1$ yr for negative velocities compared to the

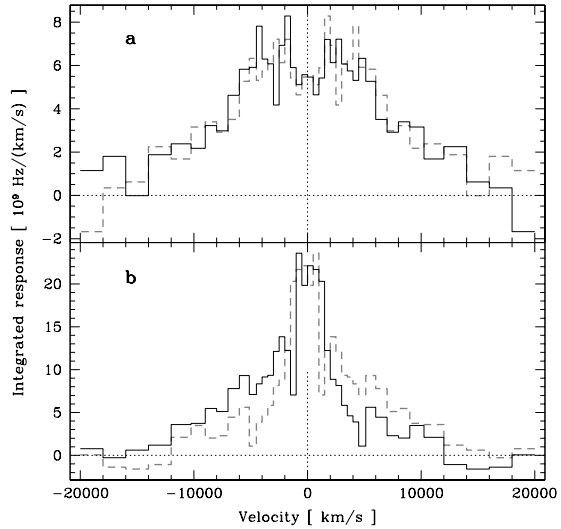


Fig. 8.— Ly α line profiles for two lag ranges. (a) Profile integrated over the range $\tau \leq 0.5$ yr. (b) Profile integrated over the range $1 \leq \tau \leq 4$ yr. In order to make the comparison between the red and blue sides easier, the grey dashed line in each panel represents the mirror of the actual profile (solid line).

positive ones.

To assess more quantitatively this latter result, we average $\Psi(\tau, v)$ over wide ranges of τ , and construct the response profiles over these ranges. We define a range corresponding to the central peak ($\tau \leq 0.5$ yr) and one extending from $\tau = 1$ up to $\tau = 4$ yr. Fig. 8 shows the two line profiles obtained this way.

The short-lag profile in Fig. 8a is very symmetrical. It is well fitted by a Gaussian with a FWHM of $\sim 18\,000 \text{ km s}^{-1}$. If left as a free parameter, the center of the Gaussian is located at a velocity of -260 km s^{-1} , a value not significantly different from zero.

The long-lag profile in Fig. 8b is however quite asymmetrical. Two important features emerge from this profile: First there are large velocities ($\sim 10\,000 \text{ km s}^{-1}$ or more) contributing to the blue wing of the profile. Second, the red wing drops sharply at velocities of the order of 1500 km s^{-1} already. The peak around 6000 km s^{-1} , very close to the location of the NV emission line, is proba-

bly not significant. We note that a contamination by N V should rather be observed in the short-lag profile, as N V should follow the continuum with a smaller lag than Ly α ; its absence in Fig. 8a shows that N V is largely negligible. Below 1500 km s⁻¹, the profile is quite symmetric.

5. Principal component analysis of the Ly α and C IV profiles

To test further the existence of the two variability modes suggested by the response function analysis, we performed a *principal component analysis* (PCA; e.g. Kendall & Stuart 1976) independently on the Ly α and C IV line profiles. Each of the 179 INES bins of the Ly α profile between 1260 and 1560 Å and of the C IV profile between 1680 and 1980 Å is extracted as a separate light curve containing 119 measurements. Each of the 119 Ly α and C IV profiles can be represented as a point in a 179-dimensional space (one axis per wavelength bin). The PCA finds an orthonormal basis in this space in which most of the coordinates of the 119 points are small. As a result, by projecting these points on the new basis vectors, we can represent the observed line profiles by a linear combination of a few characteristic line profiles determined by the PCA. In the PCA method, the new orthonormal basis is determined by the eigenvectors of the covariance matrix of the 119 × 179 matrix representing either the Ly α or C IV profiles at different times. More details on the method can be found in Türler & Courvoisier (1998).

As the response function indicates the existence of line-emitting gas responding rather quickly to the continuum, we perform the PCA on the total spectrum between 1260 and 1560 Å for Ly α and between 1680 and 1980 Å for C IV without subtracting the continuum. In this way we force the PCA to produce a line profile whose variations match very well those of the continuum. Any remaining line variability will therefore, by construction, have a light curve uncorrelated with the continuum at short lags. Fig. 9 shows the profiles (i.e. the eigenvectors) of the two main variability modes. The profiles of the first eigenvectors of Ly α and C IV are both mostly symmetric, broad bumps, with FWHM's of about 16 000 and 14 000 km s⁻¹, respectively (the spike in the C IV profile is certainly due to the reseau mark). The

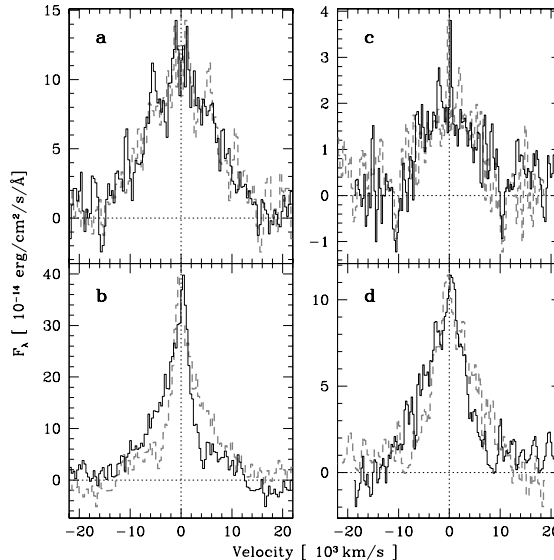


Fig. 9.— Ly α and C IV variability line profiles as obtained using the PCA. On the left, first (a) and second (b) variability modes for Ly α and on the right, first (c) and second (d) variability modes for C IV. The profiles are mirrored as in Fig. 8.

profiles of the two second eigenvectors present on the other hand an asymmetry, the red wing falling off quite faster than the blue one. The similarity of the profiles of Fig 9 with those of Fig. 8 obtained using the response function are quite remarkable, considering that the methods used to derive them are fundamentally different. Again, very little contamination by N V is observed in the Ly α profiles, except possibly at about 6000 km s⁻¹ in Fig. 9b.

For each variability mode, one can define a pseudo-light curve by projecting the individual measurements on the axis (in the 179-dimensional space) defined by the eigenvector. Fig. 10 shows three pseudo-light curves obtained this way for Ly α and C IV. As expected, the first eigenvector for Ly α produces a pseudo-light curve very similar to that of the ultraviolet continuum (Fig. 2a). The first C IV pseudo-light curve is almost identical to that of Ly α and is therefore not shown in Fig. 10. On the other hand, the pseudo-light curves of the second eigenvectors for both Ly α and C IV are characterized by variations on longer time scales dominated by the large bump between 1992 and 1996.

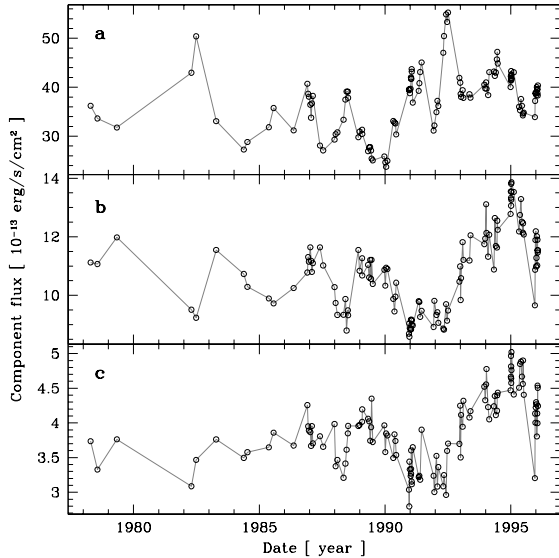


Fig. 10.— Pseudo-light curves associated with the first (a) and second (b) variability modes as obtained with the PCA for Ly α . (c) Pseudo-light curve associated with the second variability mode for CIV.

The remaining 177 eigenvectors found by the PCA have progressively smaller and smaller associated eigenvalues, which are the variances of the pseudo-light curves. This means that their associated variability modes become less and less significant. Most of these minor variability modes are expected to be white noise due to statistical fluctuations. This can be checked using a *structure function* (SF) *analysis* (e.g., Paltani 1999). We find indeed that already the third eigenvector pseudo-light curves have a nearly flat SF, which means that they are most probably dominated by statistical fluctuations.

6. Discussion

6.1. General properties

In this analysis, we have used difficult techniques, some of them (in particular the 2D response function) pushing the data to their limit. However, the use of three completely different analysis methods provide us with a way to cross-validate our results. In order to avoid overinterpretation of the data, we discuss below the results that are found to be consistent across the different

analyses. In general, the very good level of consistency show that we have really been able to gain information hidden in the light curves.

A first result from the cross-correlation analysis of the full lines, and from the 1D response function is that line response on very long time scales up to 4 yr is present in both lines. In the case of CIV, the response after $\tau \simeq 1$ yr seems even dominant. As noted above, variations on such long time scales have never been observed in previous studies of line variability in 3C 273 (Koratkar & Gaskell 1991; Kaspi et al. 2000). A simplistic, optically thin, geometrically spherical BLR model with a power-law emissivity law results in a well-defined response function: The response function is flat from $\tau = 0$ until $\tau = 2 \cdot R_{\text{in}}/c$, then decreases more or less rapidly depending on the relationship assumed between emissivity and distance, and reaches 0 for $\tau \geq 2 \cdot R_{\text{out}}/c$, R_{in} and R_{out} being respectively the inner and outer radius of the BLR (see, e.g., Fig. 1 in Pérez et al. 1992). Disregarding the bumps and hollows in the response functions (which are of questionable significance), this model requires $R_{\text{in}} \sim 0.1$ ly and $R_{\text{out}} \sim 2$ ly. The Ly α response function requires furthermore a BLR covering factor decreasing with distance with a steep power-law index $\sim 2.5 - 3$ to account for the steep decrease after the initial peak. The power-law index seems however smaller in CIV, as the decrease after the initial peak is less rapid. Such an index change would require, for instance, a stratification of metallicity, distant clouds being more metallic than nearby ones.

In both response functions, the response at $\tau = 0$ is the absolute maximum. If the line emitting medium were optically thick, emission by clouds located between the ionizing source and the observer would be strongly suppressed, and there would be very little response between $\tau = 0$ and $\tau \sim 2 \cdot R_{\text{in}}/c$. Thus the response functions indicate that the emitting medium is optically thin. Other evidences of the presence of optically thin emission medium have been pointed out, like variability properties (Shields et al. 1995), or line ratio measurements (Snedden & Gaskell 1999a,b). Further arguments are presented in Sulentic et al. (2000). Note however that Mathews (1982) finds several possible effects making an optically thick cloud radiate more or less isotropically. It is unclear however whether these effects are actually

realized.

Analyzing the line profiles, we find both evidence for symmetry at small lags and asymmetry at longer lags. The PCA analysis shows that the Ly α and C IV light curves in Fig. 2 can be interpreted as being the result of two distinct variability modes: a broad and symmetric component of the line responding quasi-simultaneously to the continuum and an asymmetric component presenting an excess in the blue wing with slower variations dominated by a large bump between 1992 and 1996. While the PCA will always separate a set of n light curves into n distinct components, the very good match between the profiles obtained with the 2D response function (Fig. 8) and those obtained with the PCA (Fig. 9) gives us strong confidence that the total Ly α and C IV lines are really formed by a combination of two separate components. The same asymmetry at long lags is also evident in the cross-correlation analysis.

Some asymmetry at small lags in the form of a small excess in the red wing is also observed in the ICCF cross-correlations. However, their absence from ZDCF cross-correlations and from the 2D response function and PCA profiles makes the reality of this effect doubtful.

In the rest of the section, we discuss separately the possible origin of these two components.

6.2. Origin of the symmetric component

The symmetric profile is easily explained in terms of non-organized velocity field, in particular Keplerian motions around a central black hole. The existence of such velocity fields in AGN has been shown by Peterson & Wandel (1999). The signature of Keplerian motions in 2D response functions is a symmetric envelope whose width decreases as $\sqrt{1/\tau}$ (where τ is the lag). This general behavior is apparent in Fig. 7, where response at lags ≤ 0.5 yr occupies a much larger velocity range than that at longer lags. Elliptical (i.e., with a continuous distribution of eccentricities between 0 and 1), rather than circular, trajectories with random inclinations seem to match best our observations, as there is little response at large velocities for very small lags in the latter case (Pérez et al. 1992; Welsh & Horne 1991). A Keplerian disk emission is also often considered as a potential source of emission lines in AGN. The accretion

disk of 3C 273 is very probably close to face-on. Superluminal velocities with $\beta_{\text{app}} \simeq 5$ (Abraham et al. 1996) indeed imply that the angle between the jet (thought to be perpendicular to the disk) and the line of sight is at most 10° . In such situation, the predicted response function is much flatter than that of a spherical shell (see Fig. 5d in Welsh & Horne 1991), which does not match well the observed response functions.

The theoretical envelopes of a 2D response function for a Keplerian circular velocity field with random inclinations for two different black-hole masses (10^8 and $10^9 M_\odot$) are shown on Fig. 7. These envelopes more or less define the observable upper and lower limits to the 2D response function of any cloud ensemble in gravitational equilibrium with random inclinations.³ While the 2D response function is too noisy to provide an accurate measurement of the black-hole mass, we note that there is significant response beyond the 10^8 - M_\odot envelope (in particular at short lags), which is evidence that a 10^9 - M_\odot black hole might be required. Because of the disk orientation, disk BLR models would require a black hole 25 times more massive than circular or elliptic models, which can probably be ruled out.

6.3. Origin of the asymmetric component

The existence of asymmetry requires that the velocity distributions on both sides of the accretion disk differ. Taken at face value, the results of the three different analyses all imply that, under the assumption that the ultraviolet continuum entirely drives the line emission, there is a significant excess of line-emitting gas animated by blue-shifted velocities from 2000 to 10 000 km s $^{-1}$ and responding with delays of a few years. This corresponds to the prediction for an infall where cloud velocity increases as clouds approach the black hole (see Fig. 2 $p = -0.5$ from Pérez et al. (1992); as the diagram is for outflowing gas, the symmetric around the $v = 0$ axis must be considered). Assuming free-fall of clouds stationary at infinite distance, it is possible to observe a given velocity for a given black-hole mass at lags 4 times larger than in the case of a circular velocity field. There-

³While clouds may in general have velocities up to the escape velocity, only a small fraction of them can be in this situation if the equilibrium condition is to be satisfied.

fore, a $10\,000\text{ km s}^{-1}$ velocity can be observed at a lag of 2 yr if the black-hole mass is about $4 \cdot 10^9 M_{\odot}$, which is slightly higher than the estimate using the symmetric part of the line. It must be noted however that infall should produce an excess of response and very strong variability at short lags for high redshifted velocities, which is not observed. Indeed, Table 2 shows that, on the contrary, the blue wings are much more variable. If the clouds were optically thick, this absence of redshifted line emission could be explained by intra-cloud obscuration masking the emission of the infalling clouds located between us and the continuum source; however, for optically thin clouds, this argument is not valid.

The ratio between short- and long-lag response is about twice as large in $\text{Ly}\alpha$ compared to C IV . To explain this difference, one would have to assume that the gas in virial motion has lower C IV emissivity compared to the free-falling gas (due, for instance, to a lower metallicity). Although this cannot be excluded, we do not see a natural scenario resulting in such a configuration.

The existence of blue-shifted, high-velocity clouds seems inescapable. However, the fact that they are found at large lags is only required under the assumption that all line emission is driven by the ultraviolet continuum. Paltani et al. (1998) performed a detailed comparison between the ultraviolet and optical continuum properties of 3C 273 using the same IUE data set as here and a very intensive optical campaign covering a large fraction of the IUE campaign. They found that, while presenting strong similarities (all peaks in the ultraviolet are found in the optical light curve), the optical light curve presents long-term variations that are absent in the ultraviolet. They concluded on the basis of spectral and polarimetric arguments that this slowly varying component (called \mathcal{R}) may be the synchrotron part of the blazar (synchrotron optical flares have been detected on several occasions in 3C 273 (Courvoisier et al. 1988)). The long-term variability properties of the line emission and of the \mathcal{R} component are remarkably similar (See Fig. 8 in Paltani et al. 1998).

If we assume that the slowly-varying line emission and the synchrotron radiation have the same origin, we readily find an explanation for the high, blue-shifted velocities: Clouds that pass in the

vicinity of the jet may be entrained by it, creating, because of the geometry of 3C 273, an outflow in the direction of the observer (clouds on the other side of the disk, which should be similarly redshifted, may be masked by the disk). Similar entrainment has been directly observed by van Breugel et al. (1985) in 3C 277.3.

Line excitation by the jet is probably not due to its ionizing radiation: The synchrotron component is much weaker than the blue-bump in the ultraviolet domain, and the Compton component emits significantly only at much higher energies. The large amount of infrared radiation emitted by the jet raises however the interesting possibility that it can be an important source of gas heating, and therefore of collisional excitation. This idea has been developed by Ma & Wills (1998), and the authors have found strong evidence that this type of excitation takes place in radio-loud quasars (Ma & Wills 2001). An important feature of this model is that C IV is much more sensitive to collisional excitation than $\text{Ly}\alpha$, which explains why the slowly varying component is comparatively much stronger in C IV than in $\text{Ly}\alpha$. The correlation with the ultraviolet continuum at large lag would either be due to a statistical coincidence in the blue-bump and synchrotron light curves, or be the result of an unknown interaction between these two components.

7. Summary and conclusion

We have presented a detailed analysis of the $\text{Ly}\alpha$ and C IV emission line properties in 3C 273. Using three different analysis methods, we find completely consistent results, namely that both $\text{Ly}\alpha$ and C IV are correlated with the ultraviolet continuum up to large lags of ~ 4 yr, that part of the lines follows quite closely the continuum variations, and that there is a strong excess of line emission at high, blue-shifted velocities (up to $10\,000\text{ km s}^{-1}$) and large lags (up to 3 yr at least). The most significant difference between $\text{Ly}\alpha$ and C IV is that, in the latter, this asymmetric excess is comparatively much stronger.

The $\text{Ly}\alpha$ and C IV response function are roughly compatible with a spherically symmetric gas distribution between a minimum distance of 0.1 yr and a maximum distance of 2 yr. We find evidence of Keplerian velocity distribution in the 2D

response function of Ly α . It is marginally possible to explain the results using two separate gas components: one with a virial velocity distribution, and one with a motion consistent with a free fall. This requires a black-hole mass of a few $10^9 M_{\odot}$. In both lines, we find evidence that the emission medium is optically thin.

We suggest however that a completely different explanation might be preferred: The high, blue-shifted velocities are the result of entrainment of the surrounding gas by the jet, and correspond therefore to outflowing gas. In this picture, the gas is collisionally excited as it is heated by the infrared radiation from the jet. This readily explains the importance of this component in C IV compared to Ly α .

An unanswered question is the relationship between the Seyfert (i.e., blue-bump) and blazar (emission from the jet) components in 3C 273. The correlation at large lag between the ultraviolet continuum and the blue-shifted line component might just be a statistical fluke, or might be the signature of a disk-jet interaction. 3C 273 proves once again to be a fundamental object for the understanding of the AGN phenomenon.

This work is supported in part (SP) by the Chandra X-ray Center under NASA contract NAS8-39073.

REFERENCES

- Abraham, Z., Carrara, E. A., Zensus, J. A., & Unwin, S. C. 1996, *A&AS*, 115, 543
- Alexander, T. 1997, in *Astronomical Time Series*, ed. D. Maoz, A. Sternberg, & E. M. Leibowitz (Dordrecht: Kluwer), 163
- Blandford, R. D. & McKee, C. F. 1982, *ApJ*, 255, 419
- Clavel, J., Reichert, G. A., Alloin, D., et al. 1991, *ApJ*, 366, 64
- Courvoisier, T. J.-L. 1998, *A&A Rev.*, 9, 1
- Courvoisier, T. J.-L., Robson, E. I., Hughes, D. H., Blecha, A., & Bouchet, P. 1988, *Nature*, 335, 330
- Dietrich, M. 1995, in *Reviews of Modern Astronomy*, Vol. 8, 235
- Gaskell, C. M. & Peterson, B. M. 1987, *ApJS*, 65, 1
- Horne, K. 1999, in *ASP Conf. Ser. 162: Quasars and Cosmology*, ed. G. Ferland & J. Baldwin (San Francisco: ASP), 189
- Kaspi, S., Smith, P. S., Netzer, H., et al. 2000, *ApJ*, 533, 631
- Kendall, M. G. & Stuart, A. 1976, *The Advanced Theory of Statistics*, 3rd edn., Vol. 3 (London: Griffin and Company)
- Koratkar, A. P. & Gaskell, C. M. 1991, *ApJS*, 75, 719
- Krolik, J. H. & Done, C. 1995, *ApJ*, 440, 166
- Ma, F. & Wills, B. J. 1998, *ApJ*, 504, L65
- . 2001, *Science*, 292, 2050
- Mathews, W. G. 1982, *ApJ*, 252, 39
- O'Brien, P. T., Goad, M. R., & Gondhalekar, P. M. 1994, *MNRAS*, 268, 845
- O'Brien, P. T. & Harries, T. J. 1991, *MNRAS*, 250, 133
- O'Brien, P. T., Zheng, W., & Wilson, R. 1989, *MNRAS*, 240, 741
- Paltani, S. 1999, in *ASP Conf. Ser. 159: BL Lac Phenomenon*, ed. L. O. Takalo & A. Sillanpää (San Francisco: ASP), 293
- Paltani, S., Courvoisier, T. J.-L., & Walter, R. 1998, *A&A*, 340, 47
- Pérez, E., Robinson, A., & de La Fuente, L. 1992, *MNRAS*, 256, 103
- Peterson, B. M. 1998, *Advances in Space Research*, 21, 57
- Peterson, B. M. & Wandel, A. 1999, *ApJ*, 521, L95
- Press, W. H., Vetterling, W. T., Teukolsky, S. A., & Flannery, B. P. 1992, *Numerical Recipes* (2nd ed.; Cambridge University Press)
- Rodríguez-Pascual, P. M., González-Riestra, R., Schartel, N., & Wamsteker, W. 1999, *A&AS*, 139, 183

- Shields, J. C., Ferland, G. J., & Peterson, B. M. 1995, *ApJ*, 441, 507
- Snedden, S. A. & Gaskell, C. M. 1999a, in *ASP Conf. Ser. 175: Structure and Kinematics of Quasar Broad Line Regions*, ed. C. M. Gaskell, W. Brandt, M. Dietrich, D. Dultzin-Hacyan, & M. Eracleous (San Francisco: ASP), 25
- Snedden, S. A. & Gaskell, C. M. 1999b, *ApJ*, 521, L91
- Sulentic, J. W., Marziani, P., & Dultzin-Hacyan, D. 2000, *ARA&A*, 38, 521
- Türler, M. & Courvoisier, T. J.-L. 1998, *A&A*, 329, 863
- Türler, M., Paltani, S., Courvoisier, T. J.-L., et al. 1999, *A&AS*, 134, 89
- Ulrich, M.-H., Courvoisier, T. J.-L., & Wamsteker, W. 1993, *ApJ*, 411, 125
- Ulrich, M.-H. & Horne, K. 1996, *MNRAS*, 283, 748
- van Breugel, W., Miley, G., Heckman, T., Butcher, H., & Bridle, A. 1985, *ApJ*, 290, 496
- Wandel, A., Peterson, B. M., & Malkan, M. A. 1999, *ApJ*, 526, 579
- Wanders, I., Goad, M. R., Korista, K. T., et al. 1995, *ApJ*, 453, L87
- Welsh, W. F. & Horne, K. 1991, *ApJ*, 379, 586
- White, R. J. & Peterson, B. M. 1994, *PASP*, 106, 879

TABLE 1

LIGHT CURVES OF THE INTEGRATED $\text{Ly}\alpha$ AND C IV EMISSION LINES. DATES ARE IN DECIMAL YEAR, AND FLUXES IN MJY FOR THE CONTINUUM AND IN UNITS OF 10^{-12} $\text{ERG S}^{-1} \text{CM}^{-2}$ FOR THE LINES.

Date	Continuum	$\text{Ly}\alpha$ Full line	C IV Full line	Blue wing		$\text{Ly}\alpha$ Core	Red wing		Blue wing	C IV Core	Red wing
				Far	Near		Near	Far			
1978.2888	11.32±0.57	20.04±1.13	4.89±0.64	2.30±0.52	2.71±0.33	8.70±0.51	3.29±0.34	3.04±0.55	0.12±0.30	4.21±0.41	0.56±0.22
1978.5627	10.40±0.36	17.90±0.76	4.89±0.50	1.78±0.33	2.70±0.24	8.36±0.42	2.88±0.23	2.18±0.34	0.38±0.19	3.79±0.40	0.72±0.14
1979.3376	8.84±0.47	17.76±1.07	5.82±0.89	1.32±0.44	2.62±0.30	8.78±0.50	3.05±0.32	2.00±0.52	1.27±0.36	3.92±0.72	0.62±0.27
1982.3021	14.24±0.32	17.12±0.68	4.63±0.35	1.35±0.30	2.60±0.19	8.11±0.29	2.86±0.19	2.20±0.31	0.54±0.19	3.65±0.17	0.44±0.14
1982.4883	17.51±0.40	18.98±0.82	5.46±0.41	0.99±0.36	2.65±0.21	8.62±0.30	3.13±0.22	3.59±0.40	0.43±0.24	4.27±0.22	0.76±0.19
1983.2867	9.77±0.56	18.38±1.07	6.36±0.68	1.38±0.47	2.59±0.31	8.76±0.47	2.96±0.33	2.68±0.54	1.13±0.36	4.09±0.43	1.15±0.30
1984.3861	8.05±0.26	16.14±0.58	5.37±0.30	0.88±0.24	2.27±0.15	7.94±0.26	2.67±0.16	2.39±0.26	1.05±0.16	3.65±0.19	0.67±0.13
1984.5287	8.86±0.33	15.55±0.69	5.86±0.42	0.74±0.29	2.34±0.20	7.71±0.36	2.71±0.22	2.05±0.31	1.33±0.23	3.82±0.23	0.71±0.17
1985.3804	9.89±0.27	16.23±0.62	5.92±0.35	1.34±0.25	2.42±0.16	7.62±0.27	2.89±0.18	1.97±0.27	1.04±0.18	3.91±0.18	0.97±0.14
1985.5698	11.59±0.44	17.70±0.92	6.00±0.46	1.32±0.40	2.42±0.26	7.97±0.43	2.98±0.27	3.01±0.43	0.87±0.27	4.09±0.24	1.04±0.21
1986.3660	9.34±0.38	15.72±0.81	5.39±0.44	1.01±0.35	2.33±0.23	7.70±0.38	2.71±0.25	1.97±0.38	0.68±0.24	3.94±0.26	0.78±0.21
1986.9123	13.69±0.36	17.75±0.84	6.63±0.39	0.95±0.35	2.77±0.21	8.59±0.34	3.08±0.22	2.36±0.35	1.09±0.22	4.61±0.23	0.93±0.16
1986.9422	12.43±0.31	18.31±0.69	6.09±0.36	1.09±0.29	2.56±0.22	9.05±0.32	3.31±0.20	2.30±0.30	0.83±0.19	4.35±0.20	0.91±0.15
1986.9751	12.25±0.32	18.39±0.69	6.29±0.40	1.44±0.30	2.50±0.19	8.76±0.32	3.30±0.20	2.39±0.31	0.93±0.20	4.27±0.20	1.09±0.22
1987.0322	11.21±0.29	19.21±0.66	6.23±0.32	1.39±0.27	2.84±0.18	8.95±0.31	3.27±0.19	2.76±0.29	0.84±0.18	4.23±0.19	1.16±0.14
1987.0619	10.51±0.30	18.31±0.62	5.73±0.36	1.56±0.27	2.57±0.18	8.49±0.29	3.13±0.19	2.55±0.29	0.73±0.19	4.06±0.20	0.93±0.16
1987.0913	11.91±0.28	18.02±0.47	5.89±0.26	1.08±0.20	2.58±0.13	8.57±0.21	3.11±0.14	2.68±0.21	0.69±0.14	4.27±0.13	0.93±0.11
1987.1331	12.30±0.31	18.87±0.65	6.29±0.32	1.15±0.27	2.63±0.18	8.82±0.32	3.41±0.20	2.86±0.30	0.88±0.18	4.21±0.18	1.20±0.14
1987.4168	8.10±0.23	17.40±0.51	5.70±0.27	1.00±0.21	2.32±0.14	8.53±0.27	2.84±0.15	2.71±0.23	0.73±0.15	4.06±0.15	0.91±0.12
1987.5424	7.83±0.23	15.60±0.55	5.49±0.29	0.76±0.21	2.29±0.15	8.04±0.27	2.65±0.16	1.86±0.24	0.77±0.16	3.81±0.16	0.90±0.12
1987.9935	9.06±0.39	15.17±0.81	5.32±0.46	0.78±0.34	2.25±0.23	7.77±0.40	2.47±0.24	1.89±0.38	0.40±0.25	4.25±0.25	0.67±0.21
1988.0369	9.54±0.39	16.10±0.79	4.93±0.47	0.79±0.33	2.00±0.22	7.75±0.38	2.84±0.25	2.72±0.38	0.57±0.26	3.66±0.26	0.70±0.21
1988.1074	10.13±0.40	14.25±0.81	4.93±0.43	0.50±0.34	1.77±0.22	7.43±0.39	2.61±0.24	1.95±0.38	0.48±0.24	3.73±0.26	0.72±0.21
1988.3511	10.87±0.28	15.52±0.56	4.93±0.32	0.95±0.24	2.02±0.15	7.51±0.26	2.61±0.17	2.44±0.27	0.49±0.17	3.61±0.19	0.83±0.14
1988.4270	12.51±0.29	17.14±0.63	5.24±0.31	1.12±0.27	2.43±0.17	8.00±0.29	3.00±0.18	2.59±0.27	0.66±0.17	3.80±0.19	0.77±0.13
1988.4735	13.44±0.47	16.92±0.86	6.06±0.47	1.25±0.40	2.18±0.25	7.61±0.40	2.97±0.27	2.91±0.42	0.67±0.27	4.13±0.26	1.26±0.22
1988.5229	12.59±0.45	18.29±0.94	6.31±0.50	1.96±0.41	2.63±0.27	7.89±0.42	3.21±0.28	2.61±0.45	0.80±0.28	4.25±0.27	1.16±0.23
1988.5328	12.48±0.39	16.59±0.85	6.58±0.43	0.77±0.36	2.26±0.22	7.73±0.35	3.04±0.25	2.78±0.42	0.98±0.25	4.38±0.22	1.22±0.20
1988.9431	8.85±0.24	16.16±0.61	5.78±0.28	0.92±0.23	2.21±0.15	8.57±0.28	2.69±0.17	1.76±0.33	0.67±0.16	4.19±0.16	0.92±0.12
1988.9901	9.62±0.28	17.22±0.65	6.30±0.35	0.88±0.27	2.57±0.17	8.19±0.27	2.95±0.18	2.64±0.28	0.96±0.18	4.22±0.20	1.13±0.15
1989.0926	9.60±0.28	16.13±0.58	6.23±0.33	0.71±0.24	2.24±0.16	8.49±0.29	2.78±0.18	1.91±0.28	0.86±0.19	4.27±0.18	1.09±0.15
1989.0958	9.54±0.25	16.82±0.55	6.74±0.31	0.77±0.22	2.28±0.15	8.17±0.28	3.00±0.17	2.61±0.25	1.04±0.20	4.47±0.16	1.24±0.13
1989.3282	7.89±0.23	15.83±0.48	5.85±0.28	0.89±0.20	2.10±0.14	8.08±0.25	2.61±0.15	2.14±0.23	0.79±0.15	4.20±0.16	0.85±0.13
1989.3694	8.43±0.23	15.74±0.49	6.04±0.27	0.99±0.20	2.13±0.14	7.93±0.26	2.70±0.15	1.98±0.22	0.76±0.15	4.25±0.16	1.03±0.12
1989.4133	8.11±0.22	16.63±0.52	5.60±0.27	0.96±0.21	2.39±0.14	8.21±0.26	2.79±0.15	2.28±0.22	0.72±0.14	3.97±0.16	0.91±0.12
1989.4515	7.91±0.23	15.49±0.54	6.00±0.28	0.68±0.22	2.08±0.14	7.79±0.25	2.73±0.16	2.21±0.24	0.77±0.15	4.15±0.17	1.08±0.13
1989.4696	7.00±0.33	16.60±0.71	6.22±0.39	1.38±0.29	2.41±0.21	7.94±0.37	2.57±0.22	2.31±0.33	1.03±0.22	4.29±0.23	0.89±0.19
1989.5114	6.99±0.21	15.36±0.48	5.68±0.26	1.20±0.19	2.11±0.13	7.65±0.25	2.47±0.14	1.93±0.22	0.80±0.14	3.94±0.15	0.94±0.12
1989.9752	7.13±0.22	16.14±0.52	5.94±0.26	1.04±0.20	2.32±0.14	7.89±0.27	2.64±0.15	2.25±0.23	0.73±0.14	4.18±0.15	1.04±0.12
1990.0139	6.84±0.33	15.37±0.71	5.48±0.40	1.06±0.30	2.11±0.20	7.52±0.35	2.54±0.22	2.12±0.33	0.55±0.22	3.85±0.22	1.08±0.19
1990.0468	6.32±0.23	15.56±0.58	5.61±0.29	1.02±0.21	2.17±0.17	7.84±0.35	2.69±0.18	1.83±0.24	0.71±0.15	3.99±0.18	0.91±0.11
1990.0983	7.17±0.22	15.07±0.49	5.81±0.26	0.56±0.19	2.16±0.14	7.90±0.27	2.38±0.15	2.06±0.22	1.03±0.15	3.87±0.15	0.91±0.12
1990.3301	10.57±0.26	16.25±0.54	5.65±0.30	1.08±0.24	2.33±0.15	7.69±0.26	2.84±0.17	2.30±0.24	0.72±0.16	3.83±0.17	1.09±0.13
1990.3771	10.30±0.41	16.99±0.82	5.98±0.46	1.27±0.36	2.39±0.24	7.50±0.37	3.08±0.26	2.76±0.40	0.82±0.26	4.08±0.25	1.08±0.22
1990.4148	10.52±0.41	16.48±0.81	6.36±0.47	1.20±0.35	2.23±0.24	7.88±0.40	3.01±0.26	2.16±0.38	1.14±0.27	4.12±0.26	1.10±0.22
1990.4448	9.34±0.25	16.39±0.55	5.24±0.28	1.13±0.23	2.33±0.15	7.96±0.27	2.87±0.16	2.10±0.24	0.60±0.15	3.80±0.16	0.83±0.12
1990.9532	13.62±0.28	15.68±0.61	5.11±0.31	1.06±0.26	2.23±0.16	7.50±0.25	2.92±0.17	1.97±0.28	0.66±0.17	3.49±0.19	0.96±0.14
1990.9673	13.65±0.29	15.29±0.65	4.80±0.33	0.82±0.27	2.18±0.16	7.79±0.26	2.77±0.17	1.72±0.28	0.66±0.18	3.28±0.17	0.85±0.14
1990.9700	13.44±0.28	15.48±0.60	5.94±0.29	1.02±0.26	2.04±0.15	7.48±0.24	2.77±0.17	1.72±0.27	1.10±0.17	3.85±0.17	0.98±0.14
1990.9886	12.68±0.46	17.57±0.97	5.47±0.57	1.95±0.43	2.41±0.27	7.60±0.43	3.09±0.29	2.52±0.44	0.76±0.30	3.81±0.27	0.90±0.24
1991.0195	13.66±0.48	16.69±1.00	5.31±0.54	1.17±0.43	2.23±0.27	7.81±0.44	2.61±0.28	2.86±0.45	0.67±0.30	3.71±0.27	0.94±0.23
1991.0349	14.51±0.36	16.55±0.76	5.14±0.40	1.03±0.33	2.37±0.20	8.01±0.33	2.94±0.21	2.21±0.33	0.52±0.22	3.69±0.21	0.93±0.17
1991.0397	14.51±0.36	16.92±0.72	5.99±0.35	1.19±0.32	2.43±0.20	7.82±0.31	2.92±0.21	2.56±0.33	0.99±0.20	3.83±0.19	1.16±0.16
1991.0447	14.40±0.35	16.96±0.78	6.18±0.37	1.22±0.34	2.69±0.21	7.81±0.31	3.07±0.21	2.16±0.33	0.80±0.21	4.14±0.20	1.24±0.17
1991.0613	15.26±0.36	16.97±0.77	5.50±0.43	0.81±0.33	2.45±0.20	8.05±0.31	2.93±0.21	2.74±0.35	0.55±0.23	3.82±0.21	1.14±0.18
1991.0647	14.87±0.33	17.83±0.72	5.68±0.34	1.31±0.31	2.71±0.19	8.02±0.30	3.06±0.20	2.73±0.32	0.89±0.19	3.75±0.19	1.04±0.14
1991.1057	12.20±0.45	16.44±0.91	5.56±0.50	1.56±0.40	2.31±0.25	7.56±0.40	2.73±0.27	2.28±0.43	0.72±0.29	4.07±0.27	0.76±0.23
1991.3434	12.74±0.46	17.52±0.94	5.79±0.48	1.18±0.40	2.25±0.26	8.16±0.43	3.24±0.29	2.69±0.45	0.59±0.27	3.93±0.25	1.26±0.23
1991.3677	14.00±0.48	18.09±0.95	5.90±0.52	1.36±0.42	2.55±0.27	8.39±0.44	3.08±0.29	2.71±0.44	0.82±0.30	3.87±0.28	1.21±0.24
1991.4009	14.70±0.48	17.38±0.99	6.01±0.55	1.42±0.44	2.68±0.28	7.95±0.43	3.17±0.30	2.15±0.46	0.94±0.30	3.79±0.28	1.28±0.24
1991.4581	15.35±0.44	19.23±0.77	6.81±0.37	1.88±0.35	2.76±0.21	8.28±0.33	3.43±0.22	2.88±0.34	1.14±0.21	4.37±0.19	1.30±0.17
1991.9333	9.83±0.26	14.99±0.64	4.87±0.29	0.85±0.26	2.10±0.17	7.11±0.29	2.53±0.17	2.40±0.27	0.68±0.17	3.52±0.16	0.67±0.13
1991.9656	9.80±0.39	16.71±0.78	4.78±0.48	1.58±0.34	2.60±0.23	7.56±0.37	2.86±0.25	2.11±0.38	0.71±0.27	3.36±0.25	0.71±0.22
1992.0479	11.38±0.42	15.61±0.82	5.85±0.44	0.63±0.35	2.42±0.25	7.45±0.39	2.78±0.26	2.32±0.40	0.85±0.27	3.95±0.24	1.05±0.21
1992.0857	12.39±0.30	16.22±0.61	5.35±0.34	0.97±0.26	2.26±0.17	7.80±0.29	2.72±0.18	2.46±0.29	0.94±0.19	3.58±0.19	0.82±0.15
1992.1243	11.88±0.43	16.57±0.84	5.48±0.49	1.34±0.37	2.24±0.25	7.59±0.40	2.92±0.26	2.49±0.41	0.89±0.28	3.85±0.26	0.74±0.22
1992.3179	15.84±0.52	19.49±1.05	5.53±0.55	2.43±0.48	2.75±0.31	8.08±0.47	3.41±0.32	2.82±0.48	0.98±0.31	3.75±0.28	0.80±0.24
1992.3456	17.83±0.56	18.41±1.07	6.00±0.57	1.09±0.49	2.71±0.32	8.25±0.47	3.28±0.32	3.07±0.51	0.80±0.33	4.01±0.30	1.18±0.25
1992.4297	19.03±0.59	22.17±1.15	5.07±0.57	2.03±0.53	3.22±0.34	9.01±0.52	4.10±0.36	3.80±0.54</			

TABLE 1—*Continued*

Date	Continuum	Ly α Full line	C IV Full line	Blue wing		Ly α Core	Red wing		Blue wing	C IV Core	Red wing
				Far	Near		Near	Far			
1994.3687	12.88±0.46	22.09±0.97	7.91±0.52	2.41±0.42	3.37±0.29	9.69±0.47	3.58±0.30	3.03±0.45	1.72±0.30	4.71±0.27	1.48±0.24
1994.4094	13.94±0.49	20.69±0.98	7.04±0.53	2.15±0.44	3.34±0.30	9.28±0.48	3.25±0.30	2.68±0.45	1.21±0.31	4.56±0.29	1.27±0.24
1994.4534	15.23±0.51	22.23±1.03	6.57±0.56	2.65±0.47	3.58±0.31	9.34±0.46	3.56±0.31	3.10±0.47	1.07±0.32	4.55±0.30	0.95±0.25
1994.4676	15.10±0.37	22.01±0.79	7.47±0.38	1.94±0.34	3.45±0.23	9.92±0.36	3.71±0.23	2.99±0.36	1.47±0.22	4.75±0.20	1.25±0.17
1994.4885	14.35±0.49	21.40±0.97	7.59±0.51	1.84±0.43	3.61±0.31	9.60±0.48	3.31±0.30	3.03±0.45	1.33±0.31	4.78±0.28	1.48±0.24
1994.9970	11.78±0.30	21.24±0.71	7.38±0.37	1.92±0.29	3.34±0.20	9.54±0.33	3.69±0.21	2.75±0.31	1.52±0.21	4.70±0.20	1.16±0.16
1995.0084	12.81±0.21	22.21±0.54	7.53±0.26	2.14±0.21	3.52±0.14	10.22±0.23	3.57±0.14	2.76±0.23	1.44±0.14	4.95±0.14	1.15±0.11
1995.0122	12.31±0.26	22.75±0.58	7.50±0.32	2.55±0.24	3.61±0.17	10.04±0.27	3.56±0.17	2.98±0.27	1.31±0.18	5.09±0.17	1.10±0.15
1995.0170	12.76±0.27	22.24±0.58	7.67±0.31	2.06±0.25	3.63±0.18	9.86±0.28	3.69±0.18	3.01±0.27	1.46±0.18	5.06±0.16	1.15±0.16
1995.0187	13.41±0.51	22.43±1.03	7.84±0.60	2.26±0.45	3.46±0.32	10.46±0.53	3.67±0.33	2.58±0.48	1.55±0.34	4.99±0.32	1.29±0.26
1995.0243	13.25±0.35	21.46±0.76	7.46±0.45	1.92±0.33	3.41±0.22	10.02±0.37	3.49±0.22	2.62±0.34	1.36±0.23	4.84±0.22	1.26±0.29
1995.0311	12.45±0.26	22.82±0.54	7.55±0.30	2.33±0.24	3.75±0.16	10.03±0.25	3.62±0.16	3.09±0.25	1.29±0.17	5.00±0.16	1.26±0.14
1995.0332	12.41±0.33	23.13±0.72	8.16±0.39	2.43±0.31	3.69±0.22	10.32±0.36	3.97±0.22	2.73±0.31	1.45±0.22	5.20±0.21	1.52±0.18
1995.1223	12.94±0.49	23.05±1.05	7.58±0.58	2.65±0.47	3.65±0.32	9.98±0.50	3.64±0.32	3.14±0.48	0.99±0.33	4.81±0.30	1.78±0.27
1995.3352	10.76±0.43	18.49±0.86	7.39±0.49	1.90±0.38	3.10±0.27	9.01±0.43	3.13±0.27	1.35±0.40	1.57±0.29	4.63±0.29	1.19±0.23
1995.3735	10.45±0.42	20.33±0.85	7.72±0.49	1.88±0.37	3.05±0.27	9.35±0.44	3.52±0.27	2.53±0.39	1.33±0.30	4.96±0.28	1.43±0.23
1995.4120	10.99±0.30	21.43±0.66	7.52±0.35	2.09±0.27	3.43±0.20	9.75±0.33	3.42±0.20	2.74±0.30	1.41±0.20	4.97±0.20	1.14±0.16
1995.4498	11.05±0.44	19.83±0.95	7.33±0.56	1.72±0.40	3.53±0.29	9.14±0.45	3.07±0.27	2.37±0.42	1.67±0.31	4.73±0.28	0.93±0.24
1995.4854	9.98±0.36	19.36±0.77	6.71±0.42	1.31±0.32	3.32±0.24	8.79±0.39	3.38±0.25	2.57±0.36	1.00±0.24	4.73±0.23	0.97±0.19
1995.4879	9.80±0.42	19.80±0.89	7.46±0.53	2.01±0.38	3.16±0.26	9.16±0.41	3.03±0.26	2.45±0.42	1.33±0.30	5.05±0.28	1.07±0.24
1995.5232	10.09±0.41	19.47±0.88	6.90±0.55	1.93±0.37	3.17±0.27	8.90±0.43	3.19±0.27	2.28±0.41	1.37±0.35	4.49±0.29	1.04±0.23
1995.9640	10.68±0.43	16.73±0.90	5.33±0.56	1.51±0.39	2.64±0.26	7.45±0.39	3.00±0.27	2.13±0.41	1.16±0.29	3.52±0.31	0.65±0.23
1995.9718	11.25±0.44	18.93±0.96	6.45±0.55	2.05±0.40	3.02±0.28	8.36±0.37	3.07±0.27	2.42±0.45	1.04±0.28	4.41±0.36	1.00±0.24
1995.9851	12.05±0.48	19.71±1.05	6.69±0.61	1.22±0.45	3.07±0.29	9.12±0.46	3.06±0.30	3.24±0.49	1.55±0.33	4.30±0.37	0.84±0.25
1995.9984	11.82±0.52	20.51±0.96	6.64±0.53	2.07±0.41	3.13±0.29	9.26±0.45	3.57±0.29	2.47±0.43	1.37±0.30	4.43±0.28	0.85±0.24
1996.0118	12.05±0.46	20.04±0.99	7.29±0.53	1.86±0.42	3.14±0.29	8.63±0.43	3.54±0.30	2.87±0.45	1.39±0.30	4.55±0.30	1.35±0.24
1996.0255	11.93±0.45	19.71±0.91	7.10±0.56	2.15±0.40	3.01±0.28	8.72±0.42	3.17±0.28	2.66±0.43	1.43±0.30	4.48±0.31	1.19±0.24
1996.0420	12.33±0.46	20.79±0.97	5.98±0.53	2.49±0.43	3.09±0.28	9.23±0.46	3.45±0.30	2.53±0.44	1.24±0.30	4.17±0.30	0.56±0.24
1996.0585	12.42±0.46	18.32±0.94	6.73±0.55	1.79±0.41	2.94±0.28	8.53±0.42	3.28±0.29	1.77±0.44	1.40±0.30	4.33±0.30	0.99±0.24
1996.0638	11.48±0.44	21.73±0.93	5.74±0.52	3.17±0.43	3.58±0.29	8.58±0.44	3.65±0.30	2.75±0.42	1.00±0.29	4.21±0.29	0.53±0.23
1996.0693	12.20±0.46	19.20±0.96	7.57±0.53	1.59±0.42	3.16±0.29	8.78±0.45	3.60±0.30	2.07±0.44	1.42±0.30	4.75±0.29	1.40±0.24
1996.0748	11.91±0.45	19.11±0.96	7.45±0.55	1.60±0.42	3.01±0.28	8.80±0.44	3.20±0.29	2.50±0.43	1.71±0.30	4.63±0.31	1.11±0.24
1996.0807	12.72±0.47	19.61±0.99	6.82±0.58	2.04±0.43	3.13±0.29	8.99±0.46	3.33±0.30	2.11±0.46	1.26±0.31	4.56±0.33	1.00±0.25

TABLE 2
RELATIVE VARIABILITY OF THE DIFFERENT PARTS OF LY α AND C IV.

Line	Blue wing		Core	Red wing	
	Far	Near		Near	Far
Ly α	0.288	0.156	0.079	0.086	0.093
C IV		0.224	0.083		0.134